Reflection and Transmission of Waves at a Fluid/Porous-Medium Interface

Arthur I.M. Denneman, Guy G. Drijkoningen, David M.J. Smeulders, and Kees Wapenaar

Centre for Technical Geoscience, Delft University of Technology, P.O. Box 5028, 2600 GA Delft, The Netherlands. E-mail: adnn@cbs.nl or a.i.m.denneman@ctg.tudelft.nl; g.g.drijkoningen@ctg.tudelft.nl; d.m.j.smeulders@ctg.tudelft.nl; c.p.a.wapenaar@ctg.tudelft.nl.

ABSTRACT

We study the wave properties at a fluid/porous-medium interface by using newly derived closed-form expressions for the reflection and transmission coefficients. We illustrate the usefulness of these relatively simple expressions by applying them to a water/porous-medium interface (with open-pore or sealed-pore boundary conditions), where the porous medium consists of (i) a water-saturated clay/silt-layer, (ii) a water-saturated sand-layer, (iii) an air-filled clay/silt-layer, or (iv) an air-filled sand-layer. We observe in the frequency range 5 Hz – 20 kHz that the fast P-wave and S-wave velocities in the four porous materials are indistinguishable from the corresponding frequency-independent ones calculated using Gassmann relations. Consequently, for these frequencies we would expect that the reflection and transmission coefficients for the four water/porous-medium interfaces are similar to the ones for corresponding interfaces between water and effective elastic media (described by Gassmann wave velocities). We observe that this expectation is not fulfilled in case of an interface between water and an air-filled porous layer with open pores. A close examination of the expressions for the reflection and transmission coefficients shows that this unexpected result is due to the large density difference between water and air.

According to Biot's theory (1956a; 1956b) three different types of waves may propagate through an isotropic, homogeneous porous material: a fast P-wave, a slow P-wave, and a S-wave. The strong predictive power of Biot's theory has been confirmed extensively in the many experiments performed the past forty years. For instance, the slow P-wave is not only observed at ultrasonic frequencies in synthetic materials [sintered glass beads; (Plona, 1980)], but also in natural air-filled sandstone (Nagy et al., 1990) and in natural water-saturated sandstone (Kelder and Smeulders, 1997). Note that these slow P-waves are generated at a fluid/porous-medium interface with open-pore boundary conditions; actually, experimental results of Rasolofosaon (1988) show that it is hard to generate slow P-waves in case of sealed-pore boundary conditions.

At a fluid/porous-medium interface an incident P-wave in the fluid is converted simultaneously into a reflected P-wave, a transmitted fast P-wave, a transmitted slow P-wave, and a transmitted S-wave. In case of normal incidence the corresponding reflection and transmission coefficients were obtained by Geertsma and Smit (1961) and Deresiewicz and Rice (1964); a summary of their results can be found in the book of Bourbié et al. (1987). For the more complicated case of oblique incidence Wu et al. (1990) presented results focusing on the dependency of the reflection and transmission coefficients on the specific type of boundary conditions (open or sealed pores); in fact, their work [based upon initial work of Feng and Johnson (1983a; 1983b)] confirmed the above mentioned experimental observation of Rasolofosaon (1988). Similar results for the fluid/porous-medium interface were obtained by Santos et al. (1992), Albert (1993), and Cieszko and Kubik (1998). The results of Santos et al. (1992) show clearly the frequency dependency of the reflection and transmission coefficients and the paper of Albert (1993) considers the two interfaces "air/air-filled porous medium" and "water/water-saturated porous medium". The paper of Cieszko and Kubik (1998) considers a porous-medium with a skeleton consisting of incompressible

material. We further note that interesting results can be found in the Ph.D. thesis of Kelder (1998) and in the French papers of Rasolofosaon and Coussy (1985a; 1985b; 1986).

To calculate the reflection and transmission coefficients for an interface between a fluid and a porous-medium, we use the boundary conditions of Deresiewicz and Skalak (1963). In the scientific publications mentioned before it is shown that these boundary conditions lead to a set of four linear equations with the reflection and transmission coefficients as the four unknowns. Closed-form expressions for these coefficients can be obtained straightforwardly by applying Cramer's rule (each coefficient is then equal to the ratio of two determinants of two different 4×4 matrices). However, in case of oblique incidence the resulting closed-form expressions are quite complicated (Feng and Johnson, 1983b; Wu et al., 1990; Kelder, 1998). Due to this complexity it is rather difficult to acquire a good physical insight in the dependencies of these coefficients on the many measurable quantities defining the fluid/porous-medium interface.

It has recently been shown by Denneman et al. [sealed pores (2000); open pores (2001)] that it is possible to derive simplified expressions for the reflection and transmission coefficients if it is assumed that both the porous skeleton and the pore fluid are much more compressible than the skeletal solid grains themselves. This rigid-grain approximation appears to be a quite good one in many practical cases. However, for low-porosity rocks one should not use this approximation, since for this kind of materials the two bulk moduli associated with the porous skeleton and the skeletal solid grains are more or less equal to each other.

The usefulness of these rigid-grain expressions for the reflection and transmission coefficients is illustrated in this paper by applying them to a water/porous-medium interface, where four different types of porous materials are distinguished: (i) a water-saturated clay/silt-layer, (ii) a water-saturated sand-layer, (iii) an air-filled clay/silt-layer, and (iv) an air-filled sand-layer. The presented results might be useful for:

(i) (near) surface seismics (5–200 Hz), (ii) crosswell tomography (200–2000 Hz), and (iii) sonic wireline logging (2–20 kHz).

The outline of the paper is as follows. We first discuss the wave velocities in a fluid and a porous material. We then present the closed-form expressions for the reflection and transmission coefficients for a fluid/porous-medium interface as obtained by Denneman et al. [sealed pores (2000); open pores (2001)]. These expressions are used to calculate the reflection and transmission coefficients for an interface between water and a water-saturated porous layer. Next, we present the results for an interface between water and an air-filled porous layer. For convenience: Table 1 contains a list of symbols used throughout this paper.

WAVE VELOCITIES IN A FLUID AND A POROUS MATERIAL

We first consider the simple case of wave propagation through an inviscid fluid. The propagation velocity of a P-wave is then given by

$$c = \sqrt{\frac{K}{\rho}}, \tag{1}$$

where K and ρ are the bulk modulus and density of the fluid, respectively. The pressure P in a fluid can be calculated by using $P = -K\boldsymbol{\nabla}\cdot\mathbf{U}$ (for plane waves: the expression for the fluid wave displacement $\mathbf{U}$ can be found in appendix A). We further note that in an inviscid fluid the shear modulus is zero; consequently, S-waves cannot propagate through an inviscid fluid.

In the classic papers of Biot (1956a; 1956b) one finds that the pore fluid pressure $P_{\rm f}$ is given by

$$P_{\rm f} = -\frac{Q}{\phi}\,\boldsymbol{\nabla}\cdot\mathbf{U}_{\rm s} - \frac{R}{\phi}\,\boldsymbol{\nabla}\cdot\mathbf{U}_{\rm f}, \tag{2}$$

whereas the forces acting on the solid portions of unit cube of porous material is denoted by the stress tensor $\boldsymbol{\tau}$ as

$$\boldsymbol{\tau} = G\left[\boldsymbol{\nabla}\mathbf{U}_\mathrm{s} + (\boldsymbol{\nabla}\mathbf{U}_\mathrm{s})^T\right] + A(\boldsymbol{\nabla}\cdot\mathbf{U}_\mathrm{s})\boldsymbol{\delta} + Q(\boldsymbol{\nabla}\cdot\mathbf{U}_\mathrm{f})\boldsymbol{\delta}, \tag{3}$$

where $\boldsymbol{\delta}$ is a unit tensor.

In equations (2) and (3) the vectors $\mathbf{U}_\mathrm{f}$ and $\mathbf{U}_\mathrm{s}$ are the wave displacements of the pore fluid and the solid material making up the skeleton, respectively (for plane waves: the expressions for the displacements $\mathbf{U}_\mathrm{f}$ and $\mathbf{U}_\mathrm{s}$ can be found in appendix A). The generalized elastic coefficients A, Q, and R in equations (2) and (3) are related to the measurable quantities ϕ, G, K_s, K_f, and K_b as shown in appendix A. Here, ϕ is the porosity, G the shear modulus, K_s the skeletal grain bulk modulus, K_f the pore fluid bulk modulus, and K_b the jacketed bulk modulus of the porous material [or dry frame bulk modulus K_dry as defined in Mavko et al. (1998)].

It was obtained by Biot (1956a; 1956b) that three different waves may propagate in an isotropic, homogeneous porous material: a fast P-wave, a slow P-wave, and a S-wave. According to Biot's theory the S-wave velocity is given by

$$c_\mathrm{S} = \sqrt{\frac{G\rho_{22}}{a_0}} \qquad \text{with} \qquad a_0 = \rho_{11}\rho_{22} - \rho_{12}^2, \tag{4}$$

where the density terms ρ_{11}, ρ_{22}, and ρ_{12} are defined as

$$\rho_{11} = (1-\phi)\rho_\mathrm{s} - \rho_{12}, \qquad \rho_{22} = \phi\rho_\mathrm{f} - \rho_{12}, \qquad \rho_{12} = -(\alpha-1)\phi\rho_\mathrm{f}, \tag{5}$$

where ρ_f and ρ_s are the densities of the pore fluid and the solid material making up the skeleton, respectively. According to Johnson et al. (1987) the complex-valued drag coefficient α for a fluid-saturated porous material is defined as

$$\alpha = \alpha_\infty\left(1 - j\frac{\omega_\mathrm{c}}{\omega}\sqrt{1 + j\frac{1}{2}\frac{\omega}{\omega_\mathrm{c}}}\right) \qquad \text{with} \qquad \omega_\mathrm{c} = \frac{\eta\phi}{k_0\rho_\mathrm{f}\alpha_\infty}, \tag{6}$$

where α_∞ is the tortuosity (note that $\alpha_\infty \geq 1$), ω the angular frequency, k_0 the steady-state permeability, and η the steady-state shear viscosity. Note that for low frequencies ω/ω_c the interaction between the grains and the pore fluid is dominated by viscous effects and for high ω/ω_c by inertial effects. At roll-over frequency ω_c the viscous and inertial effects are of comparable magnitude.

According to Biot's theory the fast P-wave velocity $c_{\rm P1}$ and slow P-wave velocity $c_{\rm P2}$ are given by

$$c_{\rm P1}^2 = \frac{a_1 + \sqrt{a_1^2 - 4a_0a_2}}{2a_0}, \qquad c_{\rm P2}^2 = \frac{a_1 - \sqrt{a_1^2 - 4a_0a_2}}{2a_0}, \tag{7}$$

where parameter a_0 is defined in equation (4), whereas a_1 and a_2 are defined as

$$a_1 = R\rho_{11} - 2Q\rho_{12} + (A+2G)\rho_{22}, \qquad a_2 = R(A+2G) - Q^2 \tag{8}$$

with $R>0$, $A+2G>0$, and $a_2>0$.

REFLECTION AND TRANSMISSION COEFFICIENTS

At a fluid/porous-medium interface an incident P-wave in the fluid is converted simultaneously into a reflected P-wave, a transmitted fast P-wave, a transmitted slow P-wave, and a transmitted S-wave. The corresponding reflection and transmission coefficients $R^{\rm F}$, $T^{\rm P1}$, $T^{\rm P2}$, and $T^{\rm S}$ are related to the wave-amplitudes $A^{\rm I}$, $A^{\rm R}$, $A^{\rm P1}$, $A^{\rm P2}$, and $A^{\rm S}$ [see appendix A: in equations (A-1), (A-2), (A-4), and (A-5)] as follows:

$$R^{\rm F} = \frac{A^{\rm R}}{A^{\rm I}}, \qquad T^{\rm P1} = \frac{A^{\rm P1}}{A^{\rm I}}, \qquad T^{\rm P2} = \frac{A^{\rm P2}}{A^{\rm I}}, \qquad T^{\rm S} = \frac{A^{\rm S}}{A^{\rm I}}. \tag{9}$$

To find $R^{\rm F}$, $T^{\rm P1}$, $T^{\rm P2}$, and $T^{\rm S}$ we use the same boundary conditions for the fluid/porous-medium interface as used by Deresiewicz and Skalak (1963) [see also the book of Bourbié et al. (1987) and the paper of Gurevich and Schoenberg (1999)]; hence, at the boundary $z=0$:

$$U_z = \phi U_{{\rm f},z} + (1-\phi)U_{{\rm s},z}, \qquad 0 = \tau_{xz}, \tag{10}$$

$$P = P_{\rm f} + j\omega T\phi(U_{{\rm f},z} - U_{{\rm s},z}), \qquad -P = -\phi P_{\rm f} + \tau_{zz}, \tag{11}$$

where U_z, $U_{{\rm f},z}$, and $U_{{\rm s},z}$ are the z-components of the fluid displacement, pore fluid displacement, and skeletal grains displacement, respectively. The fluid pressure P can

be calculated by using $P=-K\boldsymbol{\nabla}\cdot\mathbf{U}$. The pore fluid pressure $P_{\rm f}$ and the components of stress tensor $\boldsymbol{\tau}$ (i.e., τ_{xz} and τ_{zz}) can be calculated by using equations (2) and (3).

The parameter T in equation (11) is the surface flow impedance; two limiting cases are of special interest, i.e., $T=0$ and $T\to\infty$. The open-pore case $T=0$ implies free flow of fluid across the fluid/porous-medium interface. Substitution of $T=0$ in equation (11) leads to $P=P_{\rm f}$. For the sealed-pore case $T\to\infty$ there is no fluid flow across the fluid/porous-medium interface. Substitution of $T\to\infty$ in equation (11) leads to $U_{{\rm f},z}=U_{{\rm s},z}$ $[=U_z$ by equation (10)].

It is not difficult to show that the boundary conditions given in equations (10) and (11) lead to a set of four linear equations with the coefficients $R^{\rm F}$, $T^{\rm P1}$, $T^{\rm P2}$, and $T^{\rm S}$ as the four unknowns. To acquire physical insight in the computed coefficients, closed-form expressions for $R^{\rm F}$, $T^{\rm P1}$, $T^{\rm P2}$, and $T^{\rm S}$ have been derived assuming that the skeletal grains are rigid. In this paper we only present the closed-form expressions belonging to the two limiting cases $T=0$ and $T\to\infty$; unfortunately, for the intermediate cases we were only able to derive closed-form expressions that are extremely complicated.

For the sealed-pore case ($T\to\infty$) the rigid-grain approximation leads to (Denneman et al., 2000)

$$R^{\rm F}=\frac{R_1-R_2}{R_1+R_2}, \tag{12}$$

where R_1 and R_2 are defined as

$$R_1=\Delta_1+\gamma\Delta_2, \tag{13}$$

$$R_2=\frac{\rho}{4qGc_{\rm S}^2}(q_{\rm P1}+\gamma q_{\rm P2}). \tag{14}$$

Here, the vertical slownesses q, $q_{\rm P1}$, and $q_{\rm P2}$ and the parameters γ, Δ_1, and Δ_2 are defined in appendix A and B, respectively. The corresponding transmission coefficients $T^{\rm P1}$, $T^{\rm P2}$, and $T^{\rm S}$ are given by

$$T^{\rm P1}=\frac{-\rho/G}{R_1+R_2}\left(p^2-\frac{K_{\rm P1}}{2Gc_{\rm P1}^2}\right), \tag{15}$$

$$T^{\mathrm{P2}} = \frac{-\gamma\rho/G}{R_1 + R_2}\left(p^2 - \frac{K_{\mathrm{P2}}}{2Gc_{\mathrm{P2}}^2}\right), \tag{16}$$

$$T^{\mathrm{S}} = \frac{4pqc_{\mathrm{S}}^2 R_2}{R_1 + R_2}, \tag{17}$$

where the horizontal slowness p and the effective moduli K_{P1} and K_{P2} are defined in appendix A and B, respectively.

For rigid skeletal grains and open pores ($T = 0$) the reflection coefficient R^{F} is given by (Denneman et al., 2001)

$$R^{\mathrm{F}} = \frac{R_3 - R_4}{R_3 + R_4}, \tag{18}$$

where R_3 and R_4 are defined as

$$R_3 = \Delta_3 + \frac{\gamma q_{\mathrm{P2}}\Delta_4}{q_{\mathrm{P1}}}, \tag{19}$$

$$R_4 = \frac{\phi\rho q_{\mathrm{P2}}}{\alpha\rho_{\mathrm{f}} q}(\Delta_5 + \gamma\Delta_6), \tag{20}$$

whereas the parameters Δ_3, Δ_4, Δ_5, and Δ_6 are defined in appendix B. The corresponding transmission coefficients T^{P1}, T^{P2}, and T^{S} are given by

$$T^{\mathrm{P1}} = \frac{2\Delta_8}{R_3 + R_4}, \tag{21}$$

$$T^{\mathrm{P2}} = \frac{-2\Delta_7}{R_3 + R_4}, \tag{22}$$

$$T^{\mathrm{S}} = \frac{2p(q_{\mathrm{P2}}\Delta_7 - q_{\mathrm{P1}}\Delta_8)}{R_3 + R_4}\left(p^2 - \frac{1}{2c_{\mathrm{S}}^2}\right)^{-1}, \tag{23}$$

where the parameters Δ_7 and Δ_8 are defined in appendix B.

INTERFACE BETWEEN WATER AND A WATER-SATURATED POROUS MEDIUM

The obtained results so far are illustrated by applying them to the case of an interface between water and a water-saturated porous-medium. Using core and log

data obtained from a shallow borehole near the town Huesca in Spain, we distinguish two different types of porous media: (i) a water-saturated clay/silt-layer and (ii) a water-saturated sand-layer. The parameters defining these two media are shown in Table 2. The (pore) fluid is water, which is characterized by $\eta = 0.001$ Pas, $\rho = \rho_{\rm f} = 1000$ kg m^{-3}, and $K = K_{\rm f} = 2.22$ G Pa.

The fast P-wave velocity, the slow P-wave velocity, and the S-wave velocity can be calculated by using the expressions for $c_{\rm S}$, $c_{\rm P1}$, and $c_{\rm P2}$ given by equations (4) and (7). In general, the wave velocities $c_{\rm P1}$, $c_{\rm P2}$, and $c_{\rm S}$ are complex-valued: the phase velocities are then given by $[{\rm Re}(c_{\rm P1}^{-1})]^{-1}$, $[{\rm Re}(c_{\rm P2}^{-1})]^{-1}$, and $[{\rm Re}(c_{\rm S}^{-1})]^{-1}$, whereas the corresponding attenuations are defined as ${\rm Im}(-\omega/c_{\rm P1})$, ${\rm Im}(-\omega/c_{\rm P2})$, and ${\rm Im}(-\omega/c_{\rm S})$. The results for the water-saturated clay/silt-layer and water-saturated sand-layer are shown in Figures 1 and 2.

In both figures one observes: (i) the fast P-wave velocity and S-wave velocity are weakly dependent on frequency f, (ii) the slow P-wave velocity is strongly dependent on frequency f, (iii) the roll-over frequency $f_{\rm c}$ is high compared to the frequencies used in (near) surface seismics, crosswell tomography, and sonic wireline logging (these techniques are in the frequency range 5 Hz – 20 kHz, while $f_{\rm c}$ is 4.1 MHz and 43 kHz for the clay/silt-layer and sand-layer, respectively), and (iv) for the frequency domain 5 Hz – 20 kHz the slow P-wave is strongly attenuated and it has a low phase velocity. We further note that the fast P-wave in the clay/silt-layer is much more attenuated than the one in the sand-layer. On the other hand, for rather low frequencies the S-wave in the sand-layer is much more attenuated than the one in the clay/silt-layer.

The reflection and transmission coefficients $R^{\rm F}$, $T^{\rm P1}$, $T^{\rm P2}$, and $T^{\rm S}$ for the water/porous-layer interfaces are calculated by using equations (12) and (15)–(17) in case of sealed pores and by using equations (18) and (21)–(23) in case of open pores. Note that $K_{\rm s}$ is much larger than $K_{\rm b}$ and $K_{\rm f}$ (see Table 2), which justifies the use of the rigid-grain approximation. Nevertheless, this approximation introduces a small error in the calculated values of $R^{\rm F}$, $T^{\rm P1}$, $T^{\rm P2}$, and $T^{\rm S}$. However, for

our purpose this error is negligible, since an exact calculation would not change our remarks/observations in the remainder of this section.

The seismic and wireline techniques mentioned before are in the frequency range 5 Hz – 20 kHz; consequently, we calculate R^{F}, T^{P1}, T^{P2}, and T^{S} for the frequencies 10 Hz and 10 kHz. The obtained results for an interface between water and a water-saturated clay/silt-layer are shown in Figure 3, whereas the results for an interface between water and a water-saturated sand-layer are shown in Figure 4. We have omitted the results for the transmission coefficient T^{P2} in Figures 3 and 4, since $|T^{\mathrm{P2}}|$ is much smaller than $|R^{\mathrm{F}}|$, $|T^{\mathrm{P1}}|$, and $|T^{\mathrm{S}}|$. Note that the results given in Figures 3 and 4 can easily be transformed into figures showing $|R^{\mathrm{F}}|$, $|T^{\mathrm{P1}}|$, and $|T^{\mathrm{S}}|$ as a function of incident angle θ by using the relation $\theta = \arcsin(pc)$ for the domain $|pc| \leq 1$.

One observes in Figures 3 and 4 that for $f = 10$ Hz the reflection and transmission coefficients are independent of the specific type of boundary conditions. This result is consistent with the observation that the roll-over frequencies f_{c} for the water-saturated clay/silt-layer and the water-saturated sand-layer are much higher than 10 Hz (clay/silt-layer: $f_{\mathrm{c}} = 4.1$ MHz; sand-layer: $f_{\mathrm{c}} = 43$ kHz). That is, for a sufficiently low frequency the water/porous-medium interface is similar to an interface between water and an effective elastic medium described by Gassmann wave velocities (Gassmann, 1951; White, 1983; Schön, 1996). Consequently, for $f \to 0$ the slow P-wave disappears and the coefficients R^{F}, T^{P1}, and T^{S} are equal to the ones for a fluid/elastic-medium interface (de Hoop and van der Hijden, 1983); hence, for $f \to 0$ there is no dependency on the specific type of boundary conditions.

In case of a clay/silt-layer the roll-over frequency $f_{\mathrm{c}} = 4.1$ MHz is still much higher than 10 kHz, so one observes in Figure 3 that the coefficients R^{F}, T^{P1}, and T^{S} are also for $f = 10$ kHz independent of the specific type of boundary conditions. On the other hand, for the sand-layer the roll-over frequency $f_{\mathrm{c}} = 43$ kHz is not much higher than 10 kHz, which results for $f = 10$ kHz in a difference between the open-pore and sealed-pore results as can be observed in Figure 4. These results are consistent with

the fact that the steady-state permeability k_0 in the sand-layer is roughly 50 times higher than the one in the clay/silt-layer, i.e., the higher the permeability the larger the amount of water flow across the interface with open pores, which results in a larger difference between the open-pore and sealed-pore results.

Three clear discontinuities can be observed in all the plots shown in Figures 3 and 4, i.e., for the clay/silt-layer at $pc \approx 0.52$, $pc = 1$, and $pc = 1.17$ and for the sand-layer at $pc \approx 0.52$, $pc = 1$, and $pc = 1.25$. The first discontinuity at $pc \approx 0.52$ is associated with the critical incident angle $\theta_c \approx \arcsin(0.52) \approx 35^o$ at which the transmitted fast P-wave becomes evanescent. The next discontinuity at $pc = 1$ is associated with the maximum incident angle $\theta = 90^o$ (for $pc > 1$ the incident and reflected P-waves are evanescent). At the third discontinuity ($pc \approx 1.17$ for clay/silt and $pc \approx 1.25$ for sand) the S-wave in the porous medium becomes evanescent.

In Figures 3 and 4 one also observes that the reflection and transmission coefficients are very large for $pc \approx 1.36$ (clay/silt-layer) and for $pc \approx 1.43$ (sand-layer). These two values for pc are associated with the surface wave traveling along the fluid/porous-medium interface. Actually, ignoring damping, the surface wave velocity is equal to the reciprocal of the horizontal slowness p for which the reflection and transmission coefficients are maximum; thus, the surface wave traveling along the interface between water and a water-saturated clay/silt-layer is 5 percent faster than the one traveling along the water/sand-layer interface.

The surface wave velocity can also be obtained as follows: find the horizontal slowness $p = p_0$ for which the denominator of R^{F} is zero. For the sealed-pore case and open-pore case the denominator of R^{F} is equal to $R_1 + R_2$ and $R_3 + R_4$, respectively [see equations (12)–(14) and (18)–(20)]. We note, however, that the obtained $p = p_0$ for which $R_1 + R_2 = 0$ or $R_3 + R_4 = 0$ might be complex-valued (the imaginary part of this p_0 is much smaller than the real part of this p_0). In general, $[\mathrm{Re}(p_0)]^{-1}$ is the surface wave velocity, whereas its attenuation is given by $\mathrm{Im}(-p_0\omega)$.

INTERFACE BETWEEN WATER AND AN AIR-FILLED POROUS MEDIUM

In this section we consider an interface between water and an air-filled porous-medium (instead of a water-saturated one). Analogously to the previous section we use core and log data obtained from a shallow borehole near the town Huesca in Spain and we distinguish two different types of porous media: (i) an air-filled clay/silt-layer and (ii) an air-filled sand-layer. The parameters defining these two media are shown in Table 3. The pore fluid is air and it is characterized by $\rho_f = 1.2$ kg m^{-3}, $K_f = 0.1$ MPa, and $\eta = 1.82\,10^{-5}$ Pa s.

The phase velocities and attenuations of the fast P-wave, slow P-wave, and S-wave in the air-filled clay/silt-layer and air-filled sand-layer are shown in Figures 5 and 6. One observes that the velocities of the fast and slow P-wave in the air-filled porous media are much lower than the ones in water-saturated porous media (as shown in Figures 3 and 4). One also observes that in an air-filled porous medium the attenuations of the fast P-wave and S-wave are more or less the same; in a water-saturated porous medium the S-wave is much more attenuated than the fast P-wave.

The reflection and transmission coefficients R^{F}, T^{P1}, and T^{S} for an interface between water and an air-filled porous medium are shown in Figures 7 and 8. Again, $|T^{\mathrm{P2}}|$ is much smaller than $|R^{\mathrm{F}}|$, $|T^{\mathrm{P1}}|$, and $|T^{\mathrm{S}}|$ and the results for T^{P2} are therefore omitted. We further note that for the air-filled media the exact solution for R^{F}, T^{P1}, T^{P2}, and T^{S} is equal to the corresponding rigid-grain approximation where $K_s \to \infty$. The rigid-grain approximation is now an excellent one because of the very low value of the pore fluid bulk modulus K_f (the bulk modulus of air).

The significant difference between the open-pore and sealed-pore results in Figures 7 and 8 is quite remarkable. Since the roll-over frequencies f_c are very high (clay/silt-layer: $f_c = 14.5$ MHz; sand-layer: $f_c = 287$ kHz), we would have expected that the numerically obtained R^{F}, T^{P1}, and T^{S} are equal to the ones for an interface

between water and an effective elastic medium described by Gassmann wave velocities. Consequently, for $f = 10$ Hz the open-pore results should not differ that much from the sealed-pore ones. We note, however, that for $f \ll 10$ Hz the open-pore results will ultimately approach the sealed-pore results (as expected).

The significant difference between the open-pore and sealed-pore results (as shown in Figures 7 and 8) can be explained as follows. At the water/porous-medium interface with open pores the wave displacements in water are mainly coupled to the wave displacements in air (the pore fluid). The acoustic impedance of water is much higher than the acoustic impedance of air; consequently, for the open-pore case and $f = 10$ kHz the coefficients $|T^{\mathrm{P1}}|$, $|T^{\mathrm{P2}}|$, and $|T^{\mathrm{S}}|$ are very small while $|R^{\mathrm{F}}| \approx 1$. On the other hand, in case of sealed pores the wave displacements in water are mainly coupled to wave displacements in the porous skeleton. The acoustic impedances of water and the porous skeleton are of the same order of magnitude; accordingly, the sealed-pore results differ significantly from the results for the open-pore case for which there is a large impedance difference.

To calculate R^{F}, T^{P1}, T^{P2}, and T^{S} we used the closed-form expressions given by equations (12)–(17) (sealed pores) and the ones given by equations (18)–(23) (open pores). Does a close examination of these expressions help us? Yes! That is, equation (20) tells us that the reflection and transmission coefficients for the open-pore case are clearly dependent on the density ratio ρ/ρ_{f}, while this kind of dependency is not present in any of the closed-form expressions for R^{F}, T^{P1}, T^{P2}, and T^{S} valid for the sealed-pore case.

Due to the large density difference between water and air (i.e., $\rho/\rho_{\mathrm{f}} \approx 800$) one finds by using equation (20) that $|R_4|$ is much larger than $|R_3|$ for $f = 10$ kHz. Consequently, by using equation (18) one obtains for the open-pore case: $|R^{\mathrm{F}}| \approx 1$ (see Figures 7 and 8; $f = 10$ kHz). At $f = 10$ Hz the large ratio ρ/ρ_{f} is somewhat compensated by the other terms in equation (20); hence, for the open-pore case this now leads to a reflection coefficient $|R^{\mathrm{F}}|$ that differs significantly from 1 (see Figures 7

and 8; $f = 10$ Hz). We note that the difference between the open-pore and sealed-pore results only disappears at $f \ll 10$ Hz, i.e., only at extremely small frequencies the large ratio ρ/ρ_{f} is fully compensated by the other terms in equation (20).

Finally, we show in Figure 9 that the coefficients R^{F} and T^{P1} for the open-pore case ($T = 0$) change gradually into the ones for the sealed-pore case ($T \to \infty$) if one increases the surface flow impedance T. The results for the intermediate values of T are obtained by solving numerically the set of four linear equations with the coefficients R^{F}, T^{P1}, T^{P2}, and T^{S} as the four unknowns [this set represents the four boundary conditions given in equations (10) and (11)].

CONCLUDING REMARKS

In this paper we have presented our current research on the reflection and transmission properties of waves at a fluid/porous-medium interface. We have assumed that $K_{\mathrm{b}} \ll K_{\mathrm{s}}$ and $K_{\mathrm{f}} \ll K_{\mathrm{s}}$ (the rigid-grain approximation) and we have considered two types of boundary conditions: the open-pore ones and the sealed-pore ones. For both types of boundary conditions the obtained closed-form expressions for the reflection and transmission coefficients R^{F}, T^{P1}, T^{P2}, and T^{S} are relatively simple [see equations (12), (15)–(18), and (21)–(23)]. The usefulness of these expressions has been illustrated by considering four different fluid/porous-medium interfaces. The results presented in this paper might be useful for (near) surface seismics (5–200 Hz), crosswell tomography (200–2000 Hz), and sonic wireline logging (2–20 kHz). We also believe that this paper is a good starting point for acquiring a good physical insight in the dependencies of R^{F}, T^{P1}, T^{P2}, and T^{S} on the many measurable quantities defining the fluid and the porous material.

One interesting result in this paper concerns the remarkable difference between the open-pore and sealed-pore cases in Figures 7 and 8. Since the roll-over frequencies f_{c} for the air-filled clay/silt-layer and air-filled sand-layer are both very large, one would

expect that the obtained R^{F}, T^{P1}, and T^{S} are equal to the ones for an interface between water and an effective elastic medium described by Gassmann wave velocities. This is indeed the case for an interface with sealed pores; however, an interface with open pores shows peculiar behavior due to the large difference between the acoustic impedance of water and the acoustic impedance of air (the pore fluid). Moreover, the closed-form expressions for R^{F}, T^{P1}, T^{P2}, and T^{S} given by equations (18)–(23) (open pores) show a clear dependency on the ratio $\rho/\rho_{\mathrm{f}} \gg 1$, while this ρ/ρ_{f}-dependency is not present in the closed-form expressions for the sealed-pore case given by equations (12)–(17). Note that these open-pore results for air-filled porous media suggest that it is not always a good idea to model a fluid/porous-medium interface in the way one normally does at low frequencies $f \ll f_{\mathrm{c}}$, i.e., to replace the porous medium by an effective elastic medium.

We further note that the results presented in this paper might facilitate the current research in forward and inverse surface wave analysis. The denominator of the reflection coefficient R^{F} plays a central role in the determination of the phase velocity and attenuation of the surface wave traveling along the fluid/porous-medium interface. For the sealed-pore case and open-pore case this surface-wave denominator is equal to R_1+R_2 and R_3+R_4, respectively [see equations (12)–(14) and (18)–(20)]. Hence, the surface wave velocity and its attenuation can be obtained by finding a (complex-valued) horizontal slowness $p = p_0$ for which the surface wave denominator R_1+R_2 or R_3+R_4 is zero, i.e., find a $p = p_0$ such that

$$\text{for sealed-pores:} \qquad \Delta_1 + \frac{\rho q_{\mathrm{P1}}}{4qGc_{\mathrm{S}}^2} + \gamma\left(\Delta_2 + \frac{\rho q_{\mathrm{P2}}}{4qGc_{\mathrm{S}}^2}\right) = 0, \tag{24}$$

$$\text{for open-pores:} \qquad \Delta_3 + \frac{\gamma\phi\rho q_{\mathrm{P2}}\Delta_6}{\alpha\rho_{\mathrm{f}}q} + \frac{q_{\mathrm{P2}}}{q_{\mathrm{P1}}}\left(\gamma\Delta_4 + \frac{\phi\rho q_{\mathrm{P1}}\Delta_5}{\alpha\rho_{\mathrm{f}}q}\right) = 0. \tag{25}$$

Here, the phase velocity of the surface wave is equal to $[\mathrm{Re}(p_0)]^{-1}$, whereas its attenuation in the propagation direction is equal to $\mathrm{Im}(-\omega p_0)$. We finally note that the third and fourth term in equations (24) and (25) will disappear if $f \to 0$.

ACKNOWLEDGMENTS

The work described in this paper is part of the project "Heterogeneities at different scales" within the DIOC-program "Observation of the shallow subsurface" (DIOC is the Dutch acronym of "Delft Interfaculty Research Centre").

REFERENCES

Albert, D. G., 1993, A comparison between wave propagation in water-saturated and air-saturated porous materials: J. Appl. Phys., **73**, 28–36.

Biot, M. A., and Willis, D. G., 1957, The elastic coefficients of the theory of consolidation: J. Appl. Mech., **24**, 594–601.

Biot, M. A., 1956a, Theory of propagation of elastic waves in a fluid-saturated porous solid. I. Low-frequency range: J. Acoust. Soc. Am., **28**, 168–178.

——— 1956b, Theory of propagation of elastic waves in a fluid-saturated porous solid. II. Higher frequency range: J. Acoust. Soc. Am., **28**, 179–191.

Bourbié, T., Coussy, O., and Zinszner, B., 1987, Acoustics of porous media: Gulf Publ. Co.

Cieszko, M., and Kubik, J., 1998, Interaction of elastic waves with a fluid-saturated porous solid boundary: J. Theoret. Appl. Mech., **36**, 561–580.

de Hoop, A. T., and van der Hijden, J. H. M. T., 1983, Generation of acoustic waves by an impulsive line source in a fluid/solid configuration with a plane boundary: J. Acoust. Soc. Am., **74**, 333–342.

Denneman, A. I. M., Drijkoningen, G. G., Smeulders, D. M. J., and Wapenaar, C. P. A., 2000, Reflection and transmission of waves at an impermeable interface

between a fluid and a porous medium: Fifth International Conference on Mathematical and Numerical Aspects of Wave Propagation (July 10–14, 2000, Santiago de Compostela, Spain), Soc. Ind. Appl. Math., Proceedings.

Denneman, A. I. M., Drijkoningen, G. G., Smeulders, D. M. J., and Wapenaar, C. P. A., 2001, Reflection and transmission of waves at a fluid/porous-medium boundary: IUTAM Symposium on Theoretical and Numerical Methods in Continuum Mechanics of Porous Materials (September 5–10, 1999, Stuttgart, Germany), Kluwer Academic Publishers, Proceedings.

Deresiewicz, H., and Rice, J. T., 1964, The effect of boundaries on wave propagation in a liquid-filled porous solid: V. Transmission across a plane interface: Bull. Seis. Soc. Am., **54**, 409–416.

Deresiewicz, H., and Skalak, R., 1963, On uniqueness in dynamic poroelasticity: Bull. Seis. Soc. Am., **53**, 783–788.

Feng, S., and Johnson, D. L., 1983a, High-frequency acoustic properties of a fluid/porous solid interface. I. New surface mode: J. Acoust. Soc. Am., **74**, 906–914.

——— 1983b, High-frequency acoustic properties of a fluid/porous solid interface. II. The 2D reflection Green's function: J. Acoust. Soc. Am., **74**, 915–924.

Gassmann, F., 1951, Über die Elastizität poröser Medien: Vierteljahrsschrift d. Naturf. Ges. Zürich, **96**, 1–23.

Geertsma, J., and Smit, D. C., 1961, Some aspects of elastic wave propagation in fluid-saturated porous solids: Geophysics, **26**, 169–181.

Gurevich, B., and Schoenberg, M., 1999, Interface conditions for Biot's equations of poroelasticity: J. Acoust. Soc. Am., **105**, 2585–2589.

Johnson, D. L., Koplik, J., and Dashen, R., 1987, Theory of dynamic permeability and tortuosity in fluid-saturated porous media: J. Fluid Mech., **176**, 379–402.

Kelder, O., and Smeulders, D., 1997, Observation of the Biot slow wave in water-saturated Nivelsteiner sandstone: Geophysics, **62**, 1794–1796.

Kelder, O., 1998, Frequency-dependent wave propagation in water-saturated porous media: Ph.D. thesis, Delft University of Technology.

Mavko, G., Mukerji, T., and Dvorkin, J., 1998, The rock physics handbook: Tools for seismic analysis in porous media: Cambridge Univ. Press.

Nagy, P., Adler, L., and Bonner, B., 1990, Slow wave propagation in air-filled porous materials and natural rocks: Appl. Phys. Lett., **56**, 2504–2506.

Plona, T. J., 1980, Observation of a second bulk compressional wave in a porous medium at ultrasonic frequencies: Appl. Phys. Lett., **36**, 259–261.

Rasolofosaon, N. J. P., and Coussy, O., 1985a, Propagation des ondes acoustiques dans les milieux poreux saturés: Effets d'interface (première partie): Rev. Inst. Fr. Petr., **40**, 581–594.

——— 1985b, Propagation des ondes acoustiques dans les milieux poreux saturés: Effets d'interface (deuxième partie): Rev. Inst. Fr. Petr., **40**, 785–802.

Rasolofosaon, N. J. P., and Coussy, O., 1986, Propagation des ondes acoustiques dans les milieux poreux saturés: Effets d'interface (troisième partie): Rev. Inst. Fr. Petr., **41**, 91–103.

Rasolofosaon, P. N. J., 1988, Importance of interface hydraulic condition on the generation of second bulk compressional wave in porous media: Appl. Phys. Lett., **52**, 780–782.

Santos, J., Corbero, J., Ravazzoli, C., and Hensley, J., 1992, Reflection and transmission coefficients in fluid-saturated porous media: J. Acoust. Soc. Am., **91**, 1911–1923.

Schön, J. H., 1996, Physical properties of rocks: Fundamentals and principles of petrophysics: Elsevier Science Publ. Co., Inc.

Smeulders, D. M. J., and van Dongen, M. E. H., 1997, Wave propagation in porous media containing a dilute gas-liquid mixture: Theory and experiments: J. Fluid. Mech., **343**, 351–373.

White, J. E., 1983, Underground sound: Application of seismic waves: Elsevier Science Publ. Co., Inc.

Wu, K., Xue, Q., and Adler, L., 1990, Reflection and transmission of elastic waves from a fluid-saturated porous solid boundary: J. Acoust. Soc. Am., **87**, 2349–2358.

APPENDIX A–WAVE DISPLACEMENTS IN SPACE-FREQUENCY DOMAIN

The fluid/porous-medium interface is located at $z=0$ ($z<0$: fluid; $z>0$: porous medium). The fluid displacement $\mathbf{U}$ in the x-z plane with $z<0$ is defined as

$$U_x(x,z,\omega) = pA^{\mathrm{I}} \exp\left[-j\omega(px+qz)\right] + pA^{\mathrm{R}} \exp\left[-j\omega(px-qz)\right], \tag{A-1}$$

$$U_z(x,z,\omega) = qA^{\mathrm{I}} \exp\left[-j\omega(px+qz)\right] - qA^{\mathrm{R}} \exp\left[-j\omega(px-qz)\right], \tag{A-2}$$

where A^{I} and A^{R} are the amplitudes for the incident and reflected P-waves, respectively; furthermore, p is the real-valued horizontal slowness and q the vertical slowness [$\mathrm{Re}(q)>0$ and $\mathrm{Im}(q)=0$; or $\mathrm{Re}(q)=0$ and $\mathrm{Im}(q)<0$]. The slownesses p and q are related to the propagation velocity c defined by equation (1) as follows:

$$p^2+q^2=\frac{1}{c^2}. \tag{A-3}$$

Note that p and c are related to the incident angle θ as $pc=\sin(\theta)$ for the domain $|pc|\le 1$, while for $|pc|>1$ the incident and reflected waves are evanescent (inhomogeneous waves propagating along the fluid/porous-medium interface).

The skeletal grains displacement $\mathbf{U}_{\mathrm{s}}$ in the x-z plane with $z>0$ is defined as

$$\begin{aligned} U_{\mathrm{s},x}(x,z,\omega) = {} & pA^{\mathrm{P1}} \exp\left[-j\omega(px+q_{\mathrm{P1}}z)\right] + pA^{\mathrm{P2}} \exp\left[-j\omega(px+q_{\mathrm{P2}}z)\right] \\ & - q_{\mathrm{S}}A^{\mathrm{S}} \exp\left[-j\omega(px+q_{\mathrm{S}}z)\right], \end{aligned} \tag{A-4}$$

$$\begin{aligned} U_{\mathrm{s},z}(x,z,\omega) = {} & q_{\mathrm{P1}}A^{\mathrm{P1}} \exp\left[-j\omega(px+q_{\mathrm{P1}}z)\right] + q_{\mathrm{P2}}A^{\mathrm{P2}} \exp\left[-j\omega(px+q_{\mathrm{P2}}z)\right] \\ & + pA^{\mathrm{S}} \exp\left[-j\omega(px+q_{\mathrm{S}}z)\right], \end{aligned} \tag{A-5}$$

where A^{P1}, A^{P2}, and A^{S} are the amplitudes of the fast P-wave, slow P-wave, and S-wave, respectively. The vertical slownesses q_{P1}, q_{P2}, and q_{S} (all with a nonnegative real part and a nonpositive imaginary part) are related to the horizontal slowness p and the wave velocities c_{S}, c_{P1}, and c_{P2} defined in equations (4) and (7) as follows:

$$p^2+q_{\mathrm{P1}}^2=\frac{1}{c_{\mathrm{P1}}^2}, \qquad p^2+q_{\mathrm{P2}}^2=\frac{1}{c_{\mathrm{P2}}^2}, \qquad p^2+q_{\mathrm{S}}^2=\frac{1}{c_{\mathrm{S}}^2}. \tag{A-6}$$

There is simple relation between the pore fluid displacement $\mathbf{U}_{\rm f}$ and the skeletal grains displacement $\mathbf{U}_{\rm s}$, i.e., the x and z directions of $\mathbf{U}_{\rm f}$ are also given by the right hand sides of equations (A-4) and (A-5) but with one modification: the amplitudes $A^{\rm P1}$, $A^{\rm P2}$, and $A^{\rm S}$ have to be multiplied by the factors $G^{\rm P1}$, $G^{\rm P2}$, and $G^{\rm S}$, respectively. These factors are defined as (Feng and Johnson, 1983a)

$$G^{\rm P1} = \frac{Q - c_{\rm P1}^2 \rho_{12}}{c_{\rm P1}^2 \rho_{22} - R} = \frac{A + 2G - c_{\rm P1}^2 \rho_{11}}{c_{\rm P1}^2 \rho_{12} - Q}, \tag{A-7}$$

$$G^{\rm P2} = \frac{Q - c_{\rm P2}^2 \rho_{12}}{c_{\rm P2}^2 \rho_{22} - R} = \frac{A + 2G - c_{\rm P2}^2 \rho_{11}}{c_{\rm P2}^2 \rho_{12} - Q}, \tag{A-8}$$

$$G^{\rm S} = \frac{-\rho_{12}}{\rho_{22}} = \frac{\alpha - 1}{\alpha}. \tag{A-9}$$

The generalized elastic coefficients A, Q, and R are related to measurable quantities by the following expressions (Biot and Willis, 1957):

$$A = \frac{(1-\phi)^2 K_{\rm s} K_{\rm f} - (1-\phi) K_{\rm b} K_{\rm f} + \phi K_{\rm s} K_{\rm b}}{K_{\rm f}(1 - \phi - K_{\rm b}/K_{\rm s}) + \phi K_{\rm s}} - \frac{2}{3} G, \tag{A-10}$$

$$Q = \frac{\phi K_{\rm f}(K_{\rm s}(1-\phi) - K_{\rm b})}{K_{\rm f}(1 - \phi - K_{\rm b}/K_{\rm s}) + \phi K_{\rm s}}, \tag{A-11}$$

$$R = \frac{\phi^2 K_{\rm f} K_{\rm s}}{K_{\rm f}(1 - \phi - K_{\rm b}/K_{\rm s}) + \phi K_{\rm s}}, \tag{A-12}$$

These expressions for A, Q, and R are also valid for porous materials that are not fully fluid-saturated. For an extensive discussion on partially saturated porous media we refer to the paper of Smeulders and van Dongen (1997).

APPENDIX B–SOME USEFUL EXPRESSIONS

The useful parameter γ and modified wave speeds $\xi_{\mathrm{P}1}$ and $\xi_{\mathrm{P}2}$ are defined as

$$\gamma = \frac{q_{\mathrm{P}1}\xi_{\mathrm{P}1}^2 c_{\mathrm{P}2}^2}{q_{\mathrm{P}2}\xi_{\mathrm{P}2}^2 c_{\mathrm{P}1}^2} = \frac{q_{\mathrm{P}1}}{q_{\mathrm{P}2}}\left[\frac{(K_{\mathrm{f}}/\alpha\rho_{\mathrm{f}}) - c_{\mathrm{P}2}^2}{c_{\mathrm{P}1}^2 - (K_{\mathrm{f}}/\alpha\rho_{\mathrm{f}})}\right], \tag{B-1}$$

$$\xi_{\mathrm{P}1}^2 = \left(\frac{\alpha}{\phi} - 1\right)\left[\frac{\alpha\rho_{\mathrm{f}}}{K_{\mathrm{f}}} - \frac{1}{c_{\mathrm{P}1}^2}\right]^{-1}, \tag{B-2}$$

$$\xi_{\mathrm{P}2}^2 = \left(\frac{\alpha}{\phi} - 1\right)\left[\frac{1}{c_{\mathrm{P}2}^2} - \frac{\alpha\rho_{\mathrm{f}}}{K_{\mathrm{f}}}\right]^{-1}, \tag{B-3}$$

where $|c_{\mathrm{P}2}^2| < |K_{\mathrm{f}}/\alpha\rho_{\mathrm{f}}| < |c_{\mathrm{P}1}^2|$. The parameters $\Delta_1, \ldots, \Delta_8$ are similar to the Rayleigh-wave denominator (de Hoop and van der Hijden, 1983) and they are defined as

$$\Delta_1 = p^2 q_{\mathrm{S}} q_{\mathrm{P}1} + \left(p^2 - \frac{K_{\mathrm{P}1}}{2Gc_{\mathrm{P}1}^2}\right)^2, \tag{B-4}$$

$$\Delta_2 = p^2 q_{\mathrm{S}} q_{\mathrm{P}2} + \left(p^2 - \frac{K_{\mathrm{P}2}}{2Gc_{\mathrm{P}2}^2}\right)^2, \tag{B-5}$$

$$\Delta_3 = p^2 q_{\mathrm{S}} q_{\mathrm{P}1} + \left(p^2 - \frac{1}{2c_{\mathrm{S}}^2}\right)^2, \tag{B-6}$$

$$\Delta_4 = p^2 q_{\mathrm{S}} q_{\mathrm{P}2} + \left(p^2 - \frac{1}{2c_{\mathrm{S}}^2}\right)^2, \tag{B-7}$$

$$\Delta_5 = p^2 q_{\mathrm{S}} q_{\mathrm{P}1} + \left(p^2 - \frac{K_{\mathrm{p}}}{2Gc_{\mathrm{P}1}^2}\right)^2, \tag{B-8}$$

$$\Delta_6 = p^2 q_{\mathrm{S}} q_{\mathrm{P}2} + \left(p^2 - \frac{K_{\mathrm{p}}}{2Gc_{\mathrm{P}2}^2}\right)^2, \tag{B-9}$$

$$\Delta_7 = \frac{\rho c_{\mathrm{P}2}^2}{\rho_{\mathrm{f}}\xi_{\mathrm{P}2}^2}\left[p^2 q_{\mathrm{S}} q_{\mathrm{P}1} + \left(p^2 - \frac{1}{2c_{\mathrm{S}}^2}\right)\left(p^2 - \frac{K_{\mathrm{p}}}{2Gc_{\mathrm{P}1}^2}\right)\right], \tag{B-10}$$

$$\Delta_8 = \frac{\rho c_{\mathrm{P}2}^2}{\rho_{\mathrm{f}}\xi_{\mathrm{P}2}^2}\left[p^2 q_{\mathrm{S}} q_{\mathrm{P}2} + \left(p^2 - \frac{1}{2c_{\mathrm{S}}^2}\right)\left(p^2 - \frac{K_{\mathrm{p}}}{2Gc_{\mathrm{P}2}^2}\right)\right] \tag{B-11}$$

with $K_{\mathrm{p}} = K_{\mathrm{b}} + \frac{4}{3}G$, $K_{\mathrm{P}1} = K_{\mathrm{p}} + \rho_{\mathrm{f}}\xi_{\mathrm{P}1}^2$, and $K_{\mathrm{P}2} = K_{\mathrm{p}} - \rho_{\mathrm{f}}\xi_{\mathrm{P}2}^2$.

TABLES

TABLE 1. Glossary of symbols.

Symbol	Meaning
a_0, a_1, a_2	parameters needed to calculate the velocities $c_{\rm S}$, $c_{\rm P1}$, and $c_{\rm P2}$
c	P-wave velocity in fluid
$c_{\rm S}$, $c_{\rm P1}$, $c_{\rm P2}$	velocity of S-wave, fast P-wave, and slow P-wave in porous medium
f, ω, $f_{\rm c}$, $\omega_{\rm c}$	frequency with $f = \omega/2\pi$ and roll-over frequency with $f_{\rm c} = \omega_{\rm c}/2\pi$
k_0, ϕ	steady-state permeability and porosity of porous medium
p, p_0	horizontal slowness; denominator of $R^{\rm F}$ is zero for $p = p_0$
q, $q_{\rm P1}$, $q_{\rm P2}$, $q_{\rm S}$	vertical slowness of P-wave in fluid and of waves in porous medium
x, z	coordinates in x-z plane ($z < 0$: fluid; $z > 0$: porous medium)
A, Q, R	generalized elastic coefficients for porous medium
$A^{\rm I}$, $A^{\rm R}$	wave amplitudes of the incident and reflected P-wave in fluid
$A^{\rm P1}$, $A^{\rm P2}$, $A^{\rm S}$	wave amplitudes of the transmitted waves in porous medium
$G^{\rm P1}$, $G^{\rm P2}$, $G^{\rm S}$	factors needed to calculate displacement $\mathbf{U}_{\rm f}$ from displacement $\mathbf{U}_{\rm s}$
G, $K_{\rm b}$	shear modulus and jacketed bulk modulus of porous medium
K, $K_{\rm f}$	bulk modulus of fluid and pore fluid
$K_{\rm p}$, $K_{\rm P1}$, $K_{\rm P2}$	$K_{\rm p} = K_{\rm b} + \frac{4}{3}G$, $K_{\rm P1} = K_{\rm p} + \rho_{\rm f}\xi_{\rm P1}^2$, and $K_{\rm P2} = K_{\rm p} - \rho_{\rm f}\xi_{\rm P2}^2$
$K_{\rm s}$	bulk modulus of skeletal grains in porous medium
P, $P_{\rm f}$	fluid pressure and pore fluid pressure
$R^{\rm F}$, $T^{\rm P1}$, $T^{\rm P2}$, $T^{\rm S}$	reflection and transmission coefficients
$R_1 + R_2$, $R_3 + R_4$	surface wave denominator for sealed pores and open pores
T	surface flow impedance (sealed pores: $T \to \infty$; open pores: $T = 0$)
$\mathbf{U}$, $\mathbf{U}_{\rm f}$, $\mathbf{U}_{\rm s}$	wave displacement of fluid, pore fluid, and skeletal grains
α, α_∞	drag coefficient and tortuosity of porous medium
γ, $\xi_{\rm P1}$, $\xi_{\rm P2}$	a useful parameter and two modified wave speeds

$\boldsymbol{\delta}$	unit tensor
η	steady-state shear viscosity of pore fluid
θ, $\theta_{\rm c}$	incident angle and critical incident angle
ρ, $\rho_{\rm f}$, $\rho_{\rm s}$	fluid density, pore fluid density, and skeletal grains density
ρ_{11}, ρ_{22}, ρ_{12}	Biot density terms
$\boldsymbol{\tau}$	stress tensor related to the solid portions of porous material
$\Delta_1, \ldots, \Delta_8$	eight parameters that are similar to Rayleigh-wave denominator

TABLE 2. Parameters for a clay/silt-layer and a sand-layer (obtained from a shallow borehole): porosity ϕ, skeletal grains density $\rho_{\rm s}$, skeletal grain bulk modulus $K_{\rm s}$, jacketed bulk modulus $K_{\rm b}$, shear modulus G, steady-state permeability k_0, and tortuosity α_∞. Both porous layers are below the water-table and are therefore water-saturated.

	ϕ	$\rho_{\rm s}$ ($\rm kg\,m^{-3}$)	$K_{\rm s}$ (GPa)	$K_{\rm b}$ (GPa)	G (GPa)	k_0 ($10^{-12}\,\rm m^2$)	α_∞
clay/silt	0.18	2840	30	3.0	4.1	0.007	1.0
sand	0.24	2760	40	5.8	3.4	0.390	2.3

TABLE 3. Parameters for a clay/silt-layer and a sand-layer (obtained from a shallow borehole): porosity ϕ, skeletal grains density $\rho_{\rm s}$, skeletal grain bulk modulus $K_{\rm s}$, jacketed bulk modulus $K_{\rm b}$, shear modulus G, steady-state permeability k_0, and tortuosity α_∞. Both porous layers are above the water-table and are therefore air-filled.

	ϕ	$\rho_{\rm s}$ ($\rm kg\,m^{-3}$)	$K_{\rm s}$ (GPa)	$K_{\rm b}$ (GPa)	G (GPa)	k_0 ($10^{-12}\,\rm m^2$)	α_∞
clay/silt	0.21	2840	30	3.0	4.1	0.035	1.0
sand	0.26	2760	40	5.8	3.4	0.950	2.3

FIGURES

FIG. 1. Water-saturated clay/silt-layer: phase velocity and attenuation of fast P-wave, S-wave, and slow P-wave. The roll-over frequency: $f_c = \omega_c / 2\pi = 4.1$ MHz.

FIG. 2. Water-saturated sand-layer: phase velocity and attenuation of fast P-wave, S-wave, and slow P-wave. The roll-over frequency: $f_c = \omega_c / 2\pi = 43$ kHz.

FIG. 3. Reflection/transmission at interface between water and water-saturated clay/silt-layer by using the rigid-grain approximation. Note that solid and dashed lines overlap for the major part.

FIG. 4. Reflection/transmission at interface between water and water-saturated sand-layer by using the rigid-grain approximation.

FIG. 5. Air-filled clay/silt-layer: phase velocity and attenuation of fast P-wave, S-wave, and slow P-wave. The roll-over frequency: $f_c = \omega_c / 2\pi = 14.5$ MHz.

FIG. 6. Air-filled sand-layer: phase velocity and attenuation of fast P-wave, S-wave, and slow P-wave. The roll-over frequency: $f_c = \omega_c / 2\pi = 287$ kHz.

FIG. 7. Reflection/transmission at interface between water and air-filled clay/silt-layer (no difference between exact solution and corresponding rigid-grain approximation).

FIG. 8. Reflection/transmission at interface between water and air-filled sand-layer (no difference between exact solution and corresponding rigid-grain approximation).

FIG. 9. Reflection/transmission at interface between water and air-filled sand-layer:

four different surface flow impedances T with $f = 10$ kHz (no difference between exact solution and corresponding rigid-grain approximation).

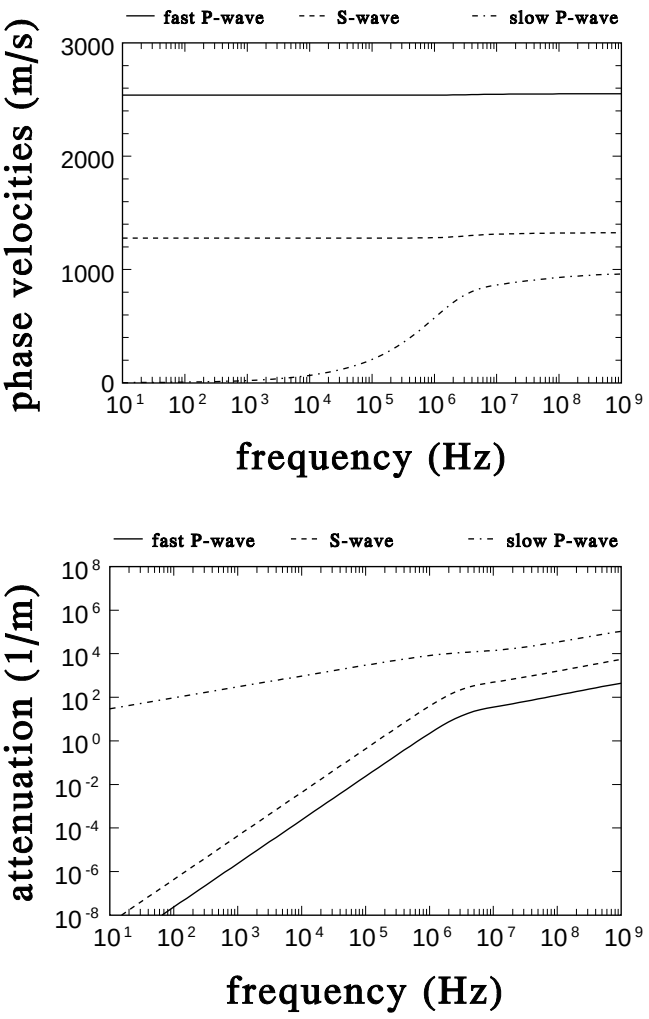

FIG. 1. Water-saturated clay/silt-layer: phase velocity and attenuation of fast P-wave, S-wave, and slow P-wave. The roll-over frequency: $f_c = \omega_c/2\pi = 4.1$ MHz.

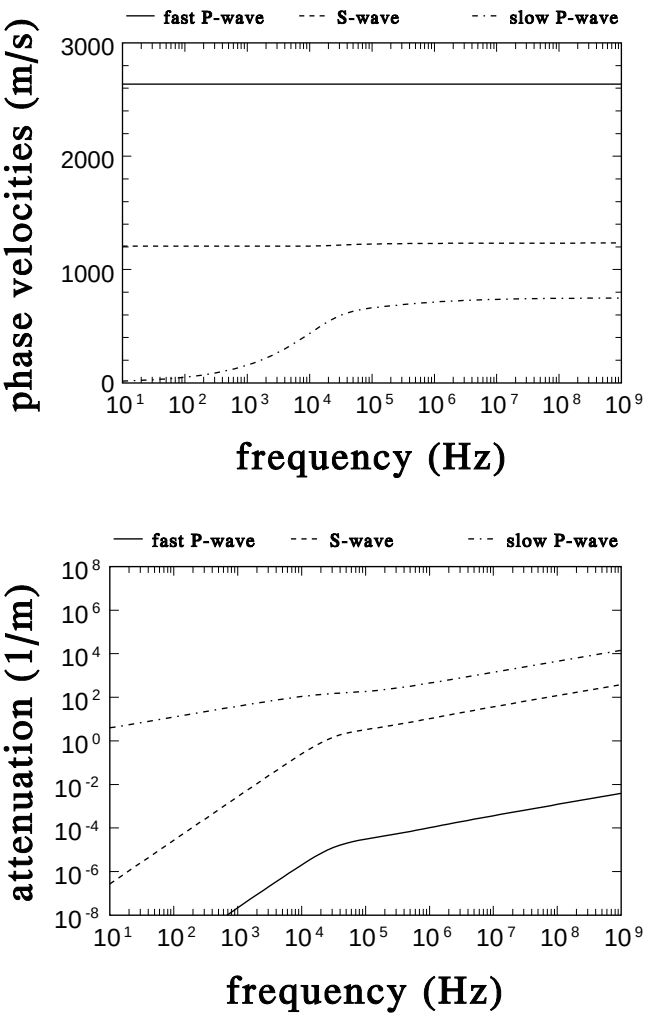

FIG. 2. Water-saturated sand-layer: phase velocity and attenuation of fast P-wave, S-wave, and slow P-wave. The roll-over frequency: $f_c = \omega_c/2\pi = 43$ kHz.

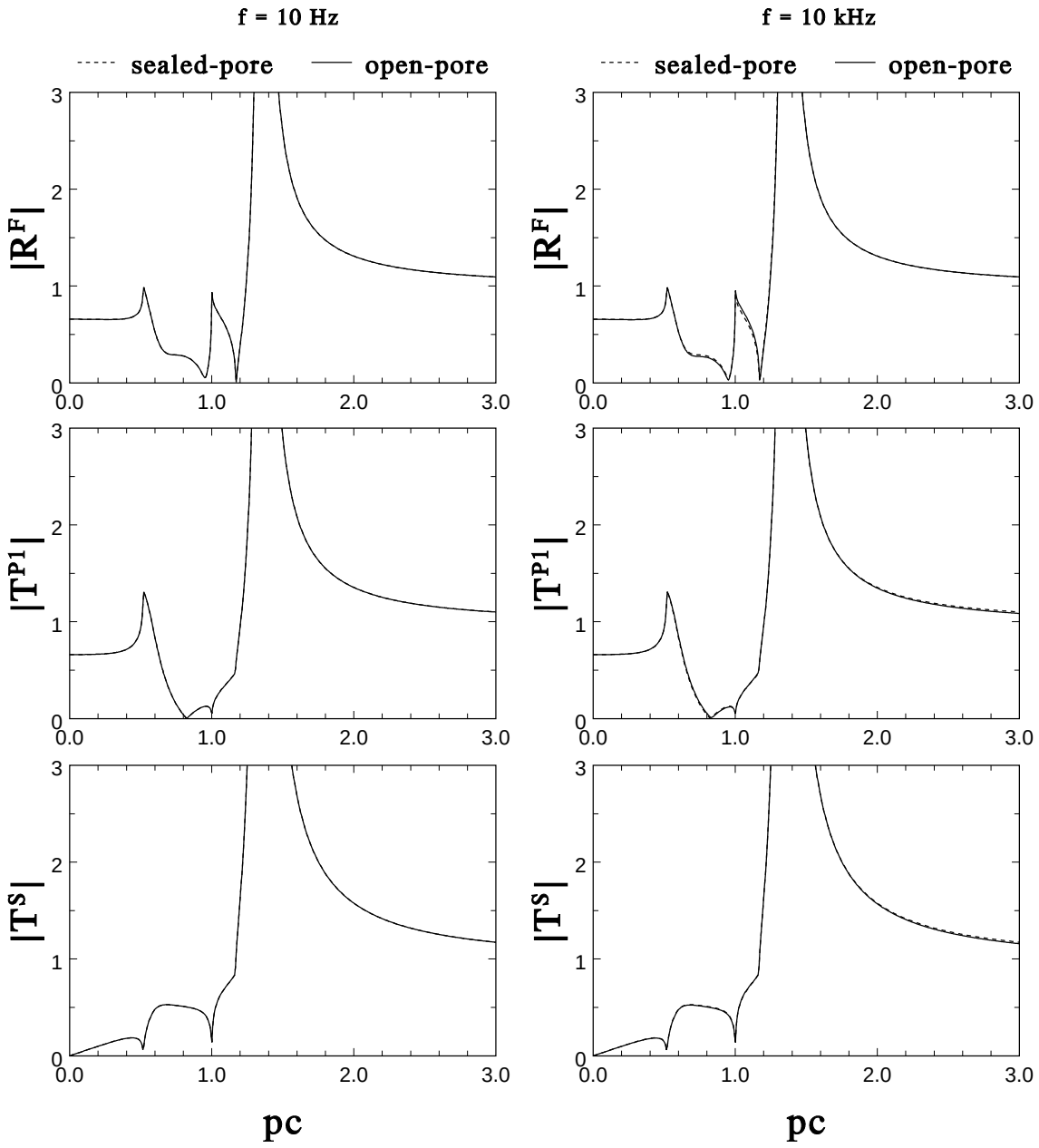

FIG. 3. Reflection/transmission at interface between water and water-saturated clay/silt-layer by using the rigid-grain approximation. Note that solid and dashed lines overlap for the major part.

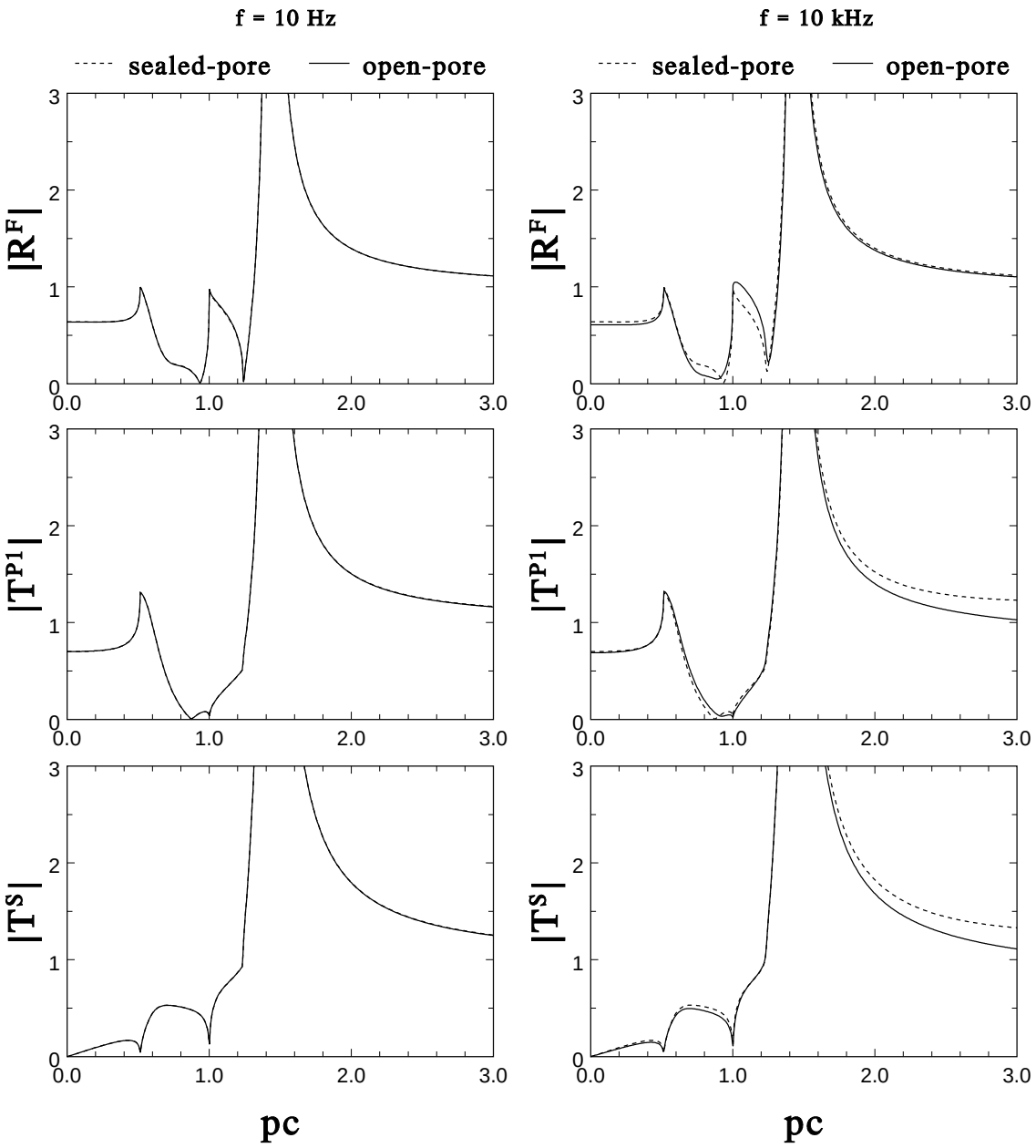

FIG. 4. Reflection/transmission at interface between water and water-saturated sand-layer by using the rigid-grain approximation.

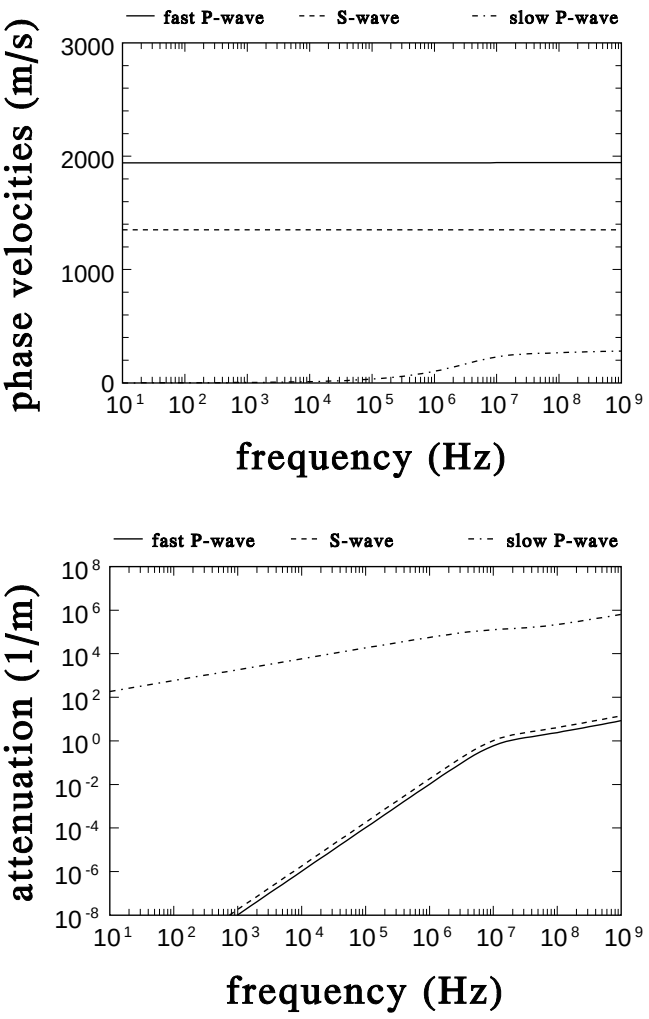

FIG. 5. Air-filled clay/silt-layer: phase velocity and attenuation of fast P-wave, S-wave, and slow P-wave. The roll-over frequency: $f_c = \omega_c/2\pi = 14.5$ MHz.

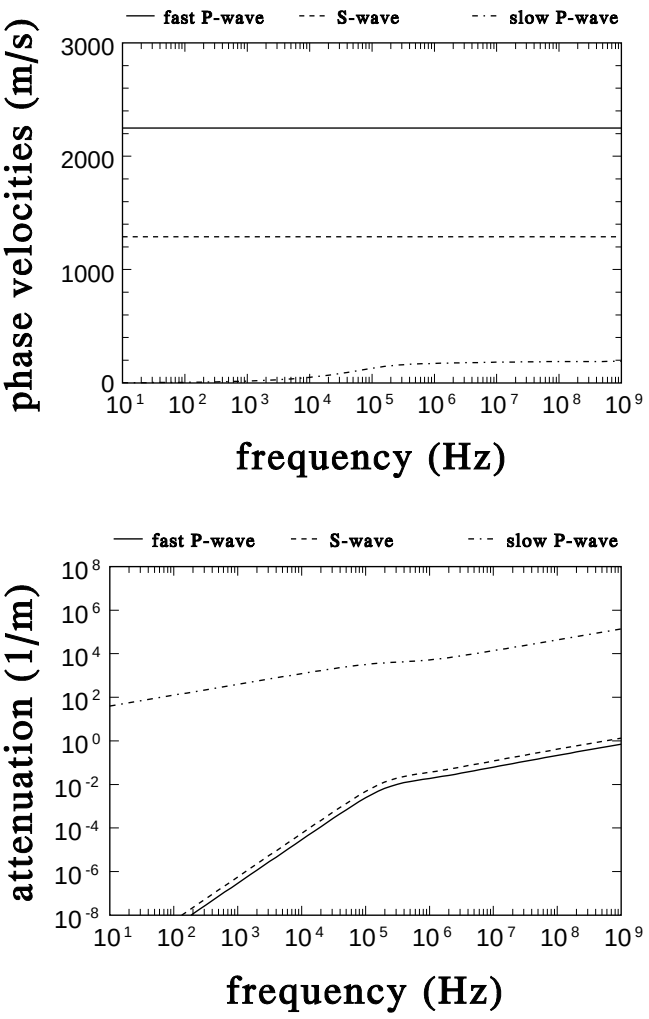

FIG. 6. Air-filled sand-layer: phase velocity and attenuation of fast P-wave, S-wave, and slow P-wave. The roll-over frequency: $f_c = \omega_c/2\pi = 287$ kHz.

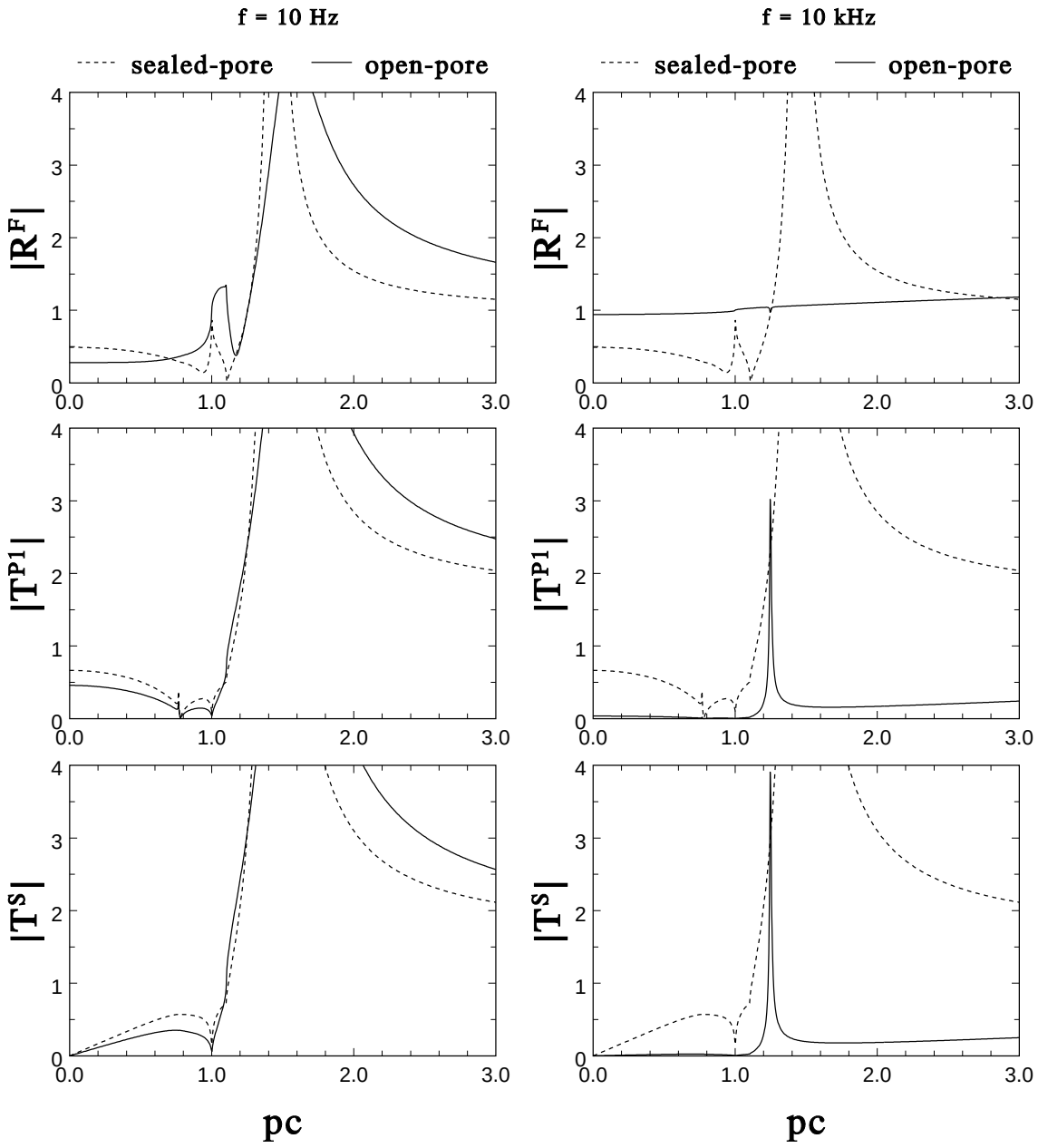

FIG. 7. Reflection/transmission at interface between water and air-filled clay/silt-layer (no difference between exact solution and corresponding rigid-grain approximation).

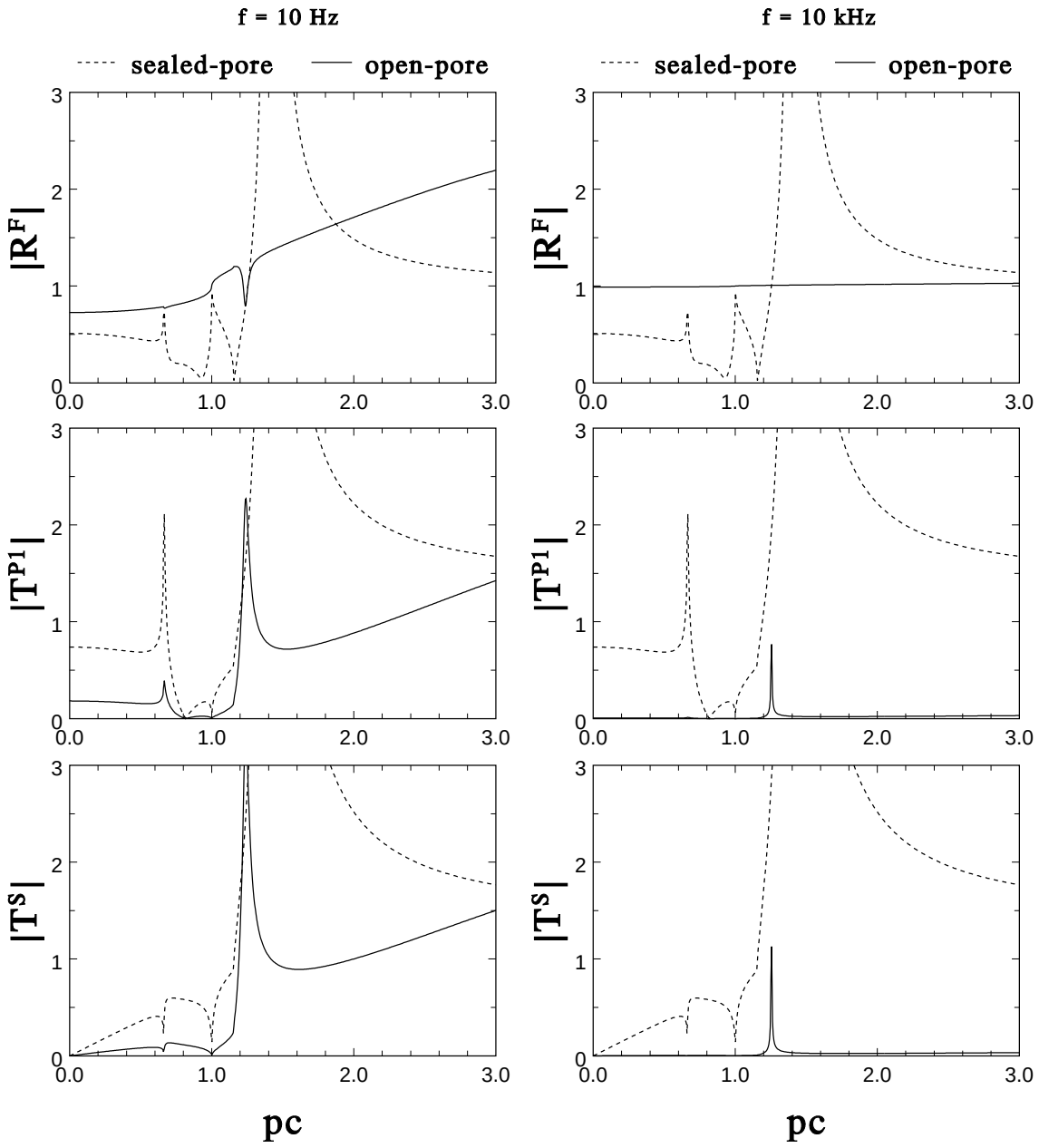

FIG. 8. Reflection/transmission at interface between water and air-filled sand-layer (no difference between exact solution and corresponding rigid-grain approximation).

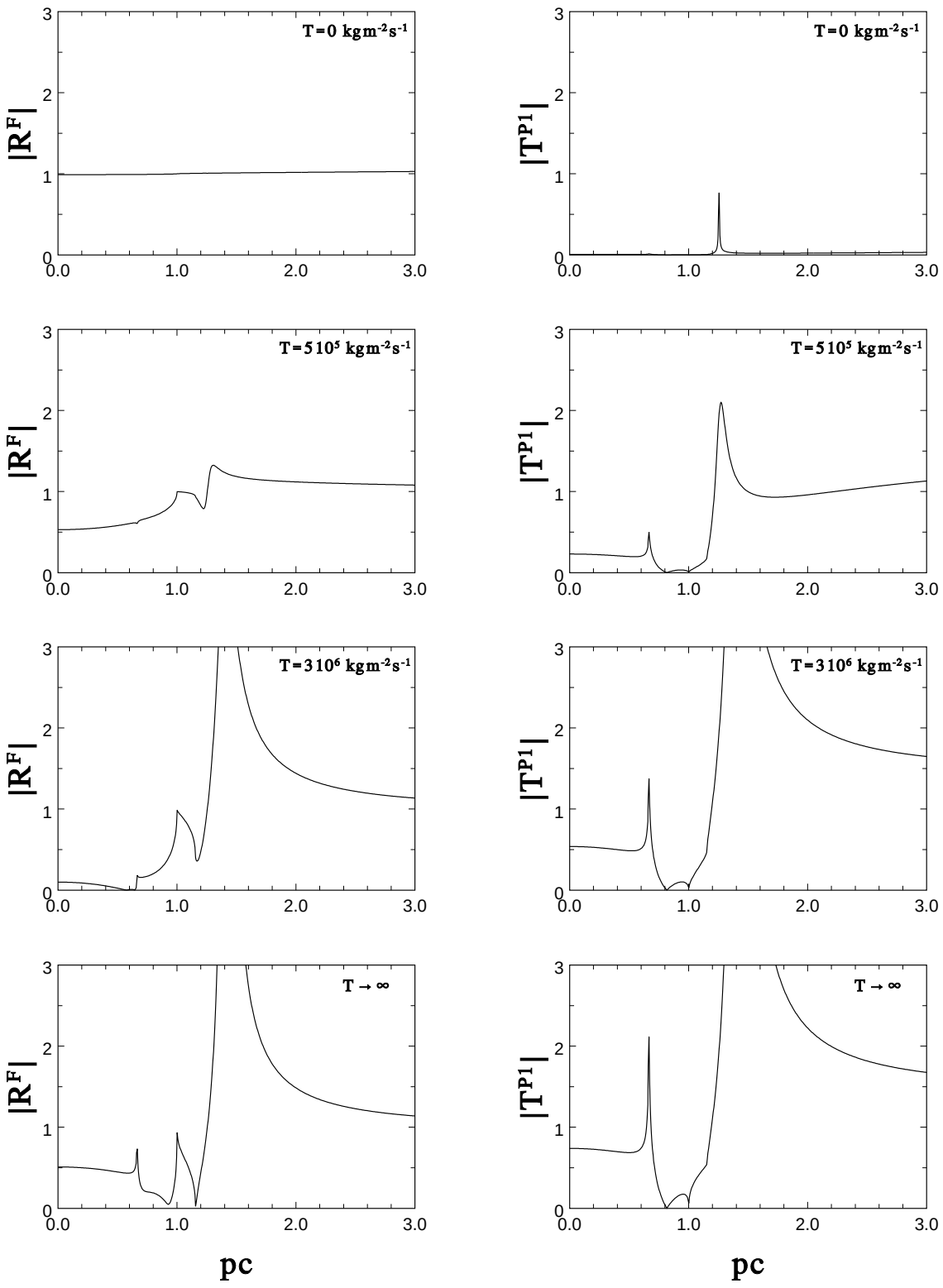
T=0 kgm-2s-1
|RF|
|TP1|
T=510^5 kgm-2s-1
T=310^6 kgm-2s-1
T → ∞
pc

FIG. 9. Reflection/transmission at interface between water and air-filled sand-layer: four different surface flow impedances T with $f = 10$ kHz (no difference between exact solution and corresponding rigid-grain approximation).